Published in Electrochimica Acta 169 (2015) 180

Magnesium Sulphide as Anode Material for Lithium-Ion Batteries

M. Helen[a,*] and Maximilian Fichtner[a,b]

[a] *Helmholtz Institute Ulm (HIU), Helmholtzstr. 11, 89081 Ulm, Germany*
[b] *Institute of Nanotechnology, Karlsruhe Institute of Technology, P.O. Box 3640, 76021 Karlsruhe, Germany*

* Corresponding author. Email address: helen.joseph@kit.edu, Tel.: +49 731 50 34215

Abstract

Herein, we report magnesium sulphide (MgS) as an anode for lithium ion batteries. Magnesium sulphide-carbon composite is directly synthesized by mechanically milling the elemental mixture. A possible lithiation and delithiation mechanism for MgS is proposed based on electrochemical and ex-situ XRD studies. The electrochemical reaction of MgS with lithium results in the formation of Li_2S and Mg, the as-formed Mg simultaneously reacts with lithium and forms Li_xMg alloy further contributing to the capacity. A stable reversible capacity of 530 mAh g^{-1} was achieved after 100 cycles within the voltage window of 0.001 - 2.5 V. The compatibility of MgS anode was tested in full cell using lithium nickel manganese cobalt oxide (LNMC) and lithium iron phosphate (LFP) as cathodes.

Key words

Magnesium sulphide; Lithium-ion battery; Full cell; Lithium nickel cobalt oxide; Lithium iron phosphate

1. Introduction

Lithium-ion batteries are commercially successful rechargeable batteries for portable electronic devices and considered promising for applications in plug-in hybrid electric vehicles. A commercial lithium-ion battery consists of, e.g., graphite anode, lithium-ion conducting electrolyte, $LiPF_6$ in ethylene carbonate-diethylcarbonate and a prelithiated cathode, $LiCoO_2$,

$LiMn_2O_4$ or $LiFePO_4$. Though metallic lithium has a theoretical specific capacity of 3,861 mAh g^{-1}, due to dendrite formation and related safety concerns alternative anodes were developed like graphite with ten times less theoretical specific capacity (372 mAh g^{-1}). Vast efforts have been made to replace graphite with high capacity anode materials [1-6]. The most promising materials are metals (Al [7,8], Sn [9-11]) and semiconductors (Si [12-14], Ge [15,16]) that can react with lithium and form alloys. In addition, a number of transition metal oxides [17-20], hydrides [21], sulphides [22,23], nitrides [24,25], and phosphides [26,27] were studied as anode for lithium-ion batteries [28]. Recently, silicon has gained much interest as it can react with more number of lithium to form a fully lithiated alloy, $Li_{4.4}Si$, with a theoretical specific capacity of 4,200 mAh g^{-1}, much higher than graphite [14]. However, it is accompanied by poor cycle life compared to graphite due to fracture and crumbling of electrode caused by large volume change (280% for Si) and due to diffusion induced stress [29]. There is a great interest for alternative high capacity, low voltage anode materials. In an attempt towards this we report the investigation of magnesium sulphide (MgS) as sustainable anode material for lithium-ion batteries.

The theoretical reaction potential of MgS with lithium is 0.5 V. It has a theoretical specific capacity of 951 mAh g^{-1} assuming the following reaction.

$$MgS + 2Li \rightarrow Li_2S + Mg$$

In addition, lithium can react with magnesium to form alloys of lithium by further increasing the theoretical capacity. The high capacity combined with low reaction potential makes MgS an interesting anode material for Li-ion batteries in principle. Hence we synthesized MgS-carbon nanocomposites and evaluated as anode material for lithium-ion batteries. Very recently, another report was published on MgS as anode for lithium-ion battery [30]. Our work is distinctive in the following aspects; 1. We report a single step preparation method of MgS carbon composite, 2. From XRD and electrochemical studies we conclude a reversible lithiation/delithiation mechanism, 3. We show that the addition of conductive carbon during electrode fabrication can significantly improve the cycling performance, 4. Further the practicality of MgS-carbon composite anode is evaluated in full cell using lithium nickel manganese cobalt oxide (LNMC) and lithium iron phosphate (LFP) as cathodes.

2. Experimental

2.1. Synthesis

Magnesium sulphide-carbon (MgS-CB) composite was prepared from the elements by ball-milling (PM100 Retsch) stoichiometric mixture (1:1 molar ratio) of magnesium powder (Alfa-Aesar, 99.8 %) and sulphur powder (Sigma-Aldrich, ≥99.5 %) with carbon black (Alfa-Aesar, >99.9 %) to obtain a mass fraction of MgS, 75 % ; carbon black, 25 %. The mixture was loaded in a tungsten carbide vial with tungsten carbide balls and closed in an argon filled glove box (MBRAUN). The ball-to-powder ratio was 10:1, milling time was 20 h at 400 rpm with 10 min milling and 10 min pause to prevent excessive heating.

2.2. Structural Characterization

X-ray diffraction (XRD) patterns were obtained with a STOE STADI P diffractometer using Cu K_α radiation in transmission mode. For ex-situ XRD studies, the powders from the current collector were retrieved and characterized at different discharged and charged states. The morphology of synthesized sample was examined by scanning electron microscopy (SEM, LEO 1550 Gemini).

2.3. Electrochemical measurements

Electrochemical studies were performed in Swagelok type cells. Electrode fabrication and assembly of electrochemical cells was done in an argon filled glove box. The electrodes were fabricated with or without additional amounts of conductive carbon. For electrodes without additional conducting carbon, the as-prepared MgS-carbon composite (75% of MgS) was mixed with the binder, poly vinylidene fluoride (PVDF) at the mass ratio of 90:10. The electrodes with conducting carbon were prepared by mixing MgS-carbon composite (75% of MgS), carbon (Super P (SP)/carbon nanofibre (CNF)/graphene (Gra)), and poly vinylidene fluoride (PVDF) in the mass ratio of 80:10:10. A slurry containing the above mixture was prepared by using N-methyl-2-pyrrolidinone as solvent, spread on a stainless steel (SS) foil (area: 1.13 cm^2), and dried in a vacuum oven at 120 °C for 12 h. Typically, each electrode contained 2−3 mg of the active material. The specific capacities were calculated based on the mass of active material in the electrode. Lithium foil (Aldrich, 99.9%) was used as the negative electrode, and a borosilicate

glass fiber sheet saturated with 1 M $LiPF_6$ in 1:1 ethylene carbonate (EC)/dimethyl carbonate (DMC) (LP30, BASF) was used as separator and electrolyte. The cells were placed in an incubator (Binder) to maintain a constant operation temperature of 25 ± 0.1 °C. Electrochemical studies were carried out using Arbin battery cycling unit BT2000 and Bio-logic VMP-3 potentiostat. Electrochemical impedance spectroscopy (EIS, Bio-logic VMP-3) measurements were performed with an applied AC signal amplitude of 10 mV over a frequency range of 200 kHz to 10 mHz.

3. Results and discussion

Various methods have been reported for the preparation of pure MgS which all require high-temperature, long sintering time and utilizing toxic chemicals as precursors. [31]. However, nanocrystalline active material (MgS) coated with carbon would be of particular interest to obtain better electrochemical performance. To achieve this, MgS-carbon composite (MgS-CB) was synthesized by mechanically milling the elemental mixture. The XRD profile of as-synthesized MgS-CB is shown in Fig. 3a. The MgS peaks are consistent with the standard JCPDS card number 35-0730 with rock salt type structure. The average crystallite size calculated by Scherer equation was 24 nm. The microstructure of the as-prepared MgS-CB was characterized by scanning electron microscopy (SEM). Fig. 1 shows the SEM image of the as-prepared MgS-CB composite and the corresponding energy dispersive X-ray spectrometry (EDS) maps of Mg, S and C. The smaller particles of MgS-CB composites were aggregated to form secondary particles in the range of 5 to 10 μm in size with irregular particle shapes. EDS indicated a homogeneous distribution of Mg, S and C in the material.

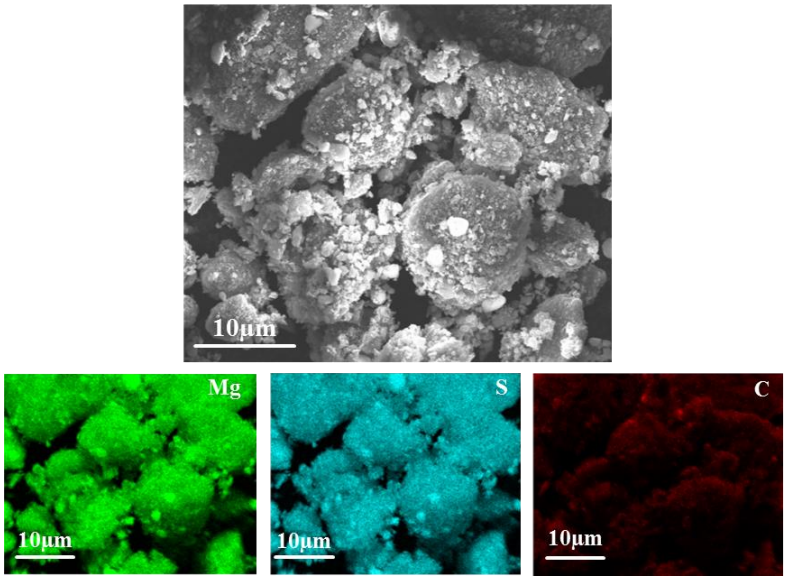

Fig. 1 SEM image of as-prepared MgS-CB and the corresponding EDS mapping of Mg, S and C.

Fig. 2a, shows the cyclic voltammogram of MgS-CB composite. The cathodic and anodic scan gives information about the discharge process (alloying or lithiation) and charge process (dealloying or lithium extraction) respectively. Two cathodic peaks centered at 0.72 V and a sharp peak at 0.005 V were observed in the first cycle. The peak at 0.72 V in the first cathodic scan disappeared in the subsequent cycles suggesting decomposition of solvent and electrolyte forming a solid-electrolyte interface (SEI). The sharp peak at 0.005 V is due to the reaction of MgS with Li (discussed below). During anodic scan, two peaks centered at 0.21 V and 0.67 V were observed. On subsequent cycling, two cathodic and anodic peaks were observed corresponding to the two step lithiation and delithiation process. The cathodic peak at 0.25 V was due to the lithiation of MgS and that observed at 0.005 V was due to the alloying of Li with Mg that is formed during the reduction of MgS [32-34]. From previous studies, alloying of Li with Mg is proved to occur below 0.1 V vs Li/Li^+ in anode materials like pure Mg [33], Mg-Ni [34], Mg_2Si [35] and Mg_2Sn [36] alloys. Two anodic peaks centered at 0.21 V and 0.67 V correspond to the delithiation process. With increasing cycle number the anodic and cathodic peaks current increases indicating a progressive activation of the material under cyclic voltammetric (CV) conditions.

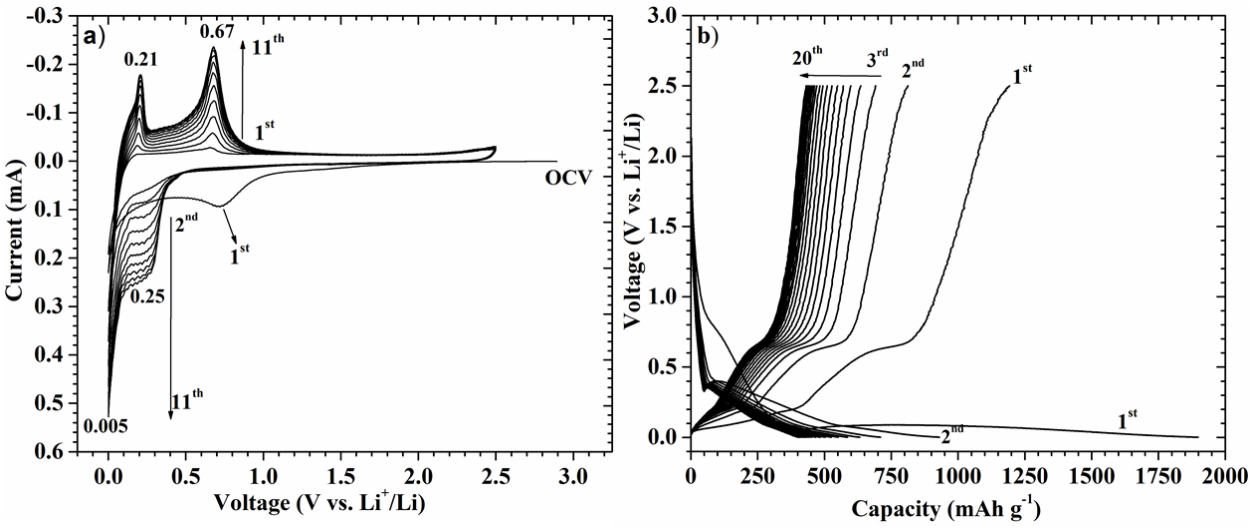

Fig. 2 Electrochemical properties of MgS-CB prepared by ball milling. (a) Cyclic voltammogram of MgS-CB at a scan rate of 0.03 mV s^{-1}. (b) The discharge and charge profiles of MgS-CB obtained at 50 mA g^{-1}.

Fig. 2b shows the electrochemical discharge and charge profiles of MgS-carbon composite anode obtained at a current density of 50 mA g^{-1}. In the first discharge, the voltage faded rapidly from the initial OCV of 2.9 V to 0.9 V followed by a monotonous fading until 0.1 V with an irreversible voltage plateau between 0.9 V and 0.5 V. This is attributed to the formation of solid electrolyte interfaces (SEI) film [37] and to the insertion of lithium into carbon, together corresponding to a capacity of 318 mAh g^{-1}. Further, a long flat plateau was observed between 0.1 - 0.001 V. The length of this plateau corresponds to a capacity of 1550 mAh g^{-1}. This plateau is due to the reaction of MgS with Li. This was corroborated by the XRD patterns collected at various discharged states (discussed below). The total discharge capacity in the first cycle was 1899 mAh g^{-1}. Upon charging, a low voltage plateau was observed at 0.21 V corresponding to a capacity of 575 mAh g^{-1} and a second plateau was observed centered at 0.67 V followed by a steep rise to the cut off voltage (2.5 V) resulting in a total charge capacity of 1194 mAh g^{-1}. An irreversible capacity loss (ICL) of 705 mAh g^{-1} was observed in the first cycle. The volume change accompanied by the conversion reaction and SEI formation in the first discharge can typically contribute to the ICL.

During second discharge, voltage rapidly faded and a sloppy region was observed between 0.4 V - 0.1 V followed by small plateau until 0.001 V (the cut off voltage) was reached. This corresponds to a capacity of 930 mAh g^{-1}. The second discharge curve was different to that of first discharge curve. The change was due to the different intermediates formed in the first charge and due to the activation of MgS in the first discharge. The second charge resembled the first charge nevertheless the total capacity was less (813 mAh g^{-1}). The subsequent discharge/charge behaviour was similar to the second discharge/charge curves. However, there was a constant capacity fading with increasing number of cycles.

In order to investigate the lithiation/delithiation mechanism during the first cycle, ex-situ XRD patterns were collected on the electrodes discharged and charged to various depths. Fig. 3b shows the XRD patterns recorded after discharging the cell to a capacity of 1180 mAh g^{-1} (by taking into account the capacity contribution from both carbon and MgS) during the first discharge. Apart from MgS peaks, Li_2S and metallic Mg peaks were observed. In addition, it is interesting to note the formation of Li alloy with Mg ($2\theta = 36.2°$, intense peak for Li_xMg) [38]. The complete reduction of MgS is expected at the recorded capacity, as the theoretical capacity of MgS is 951 mAh g^{-1}. However, peaks corresponding to MgS were still observed indicating an incomplete reaction. Further, XRD patterns were recorded for the fully discharged cell to 0.001 V (cut off voltage) and represented in Fig. 3c. The peaks due to MgS almost vanished and intensities of Li_2S, Mg, Li_xMg alloy peaks increased. Although energetically the lithiation of MgS should occur before the formation of Li_xMg alloy, due to the large overvoltage in the first reaction, lithiation of MgS can occur at 0.1 V which is close to the formation potential of Li_xMg alloy [32, 34]. Based on the XRD results and voltage-capacity profiles we propose a reaction of MgS with Li to form Li_2S and Mg. Thus the as-formed Mg is reacting with Li to form Li_xMg alloy in a subsequent reaction.

$$MgS + 2Li \longleftrightarrow Li_2S + Mg$$

$$Mg + xLi \longleftrightarrow Li_xMg$$

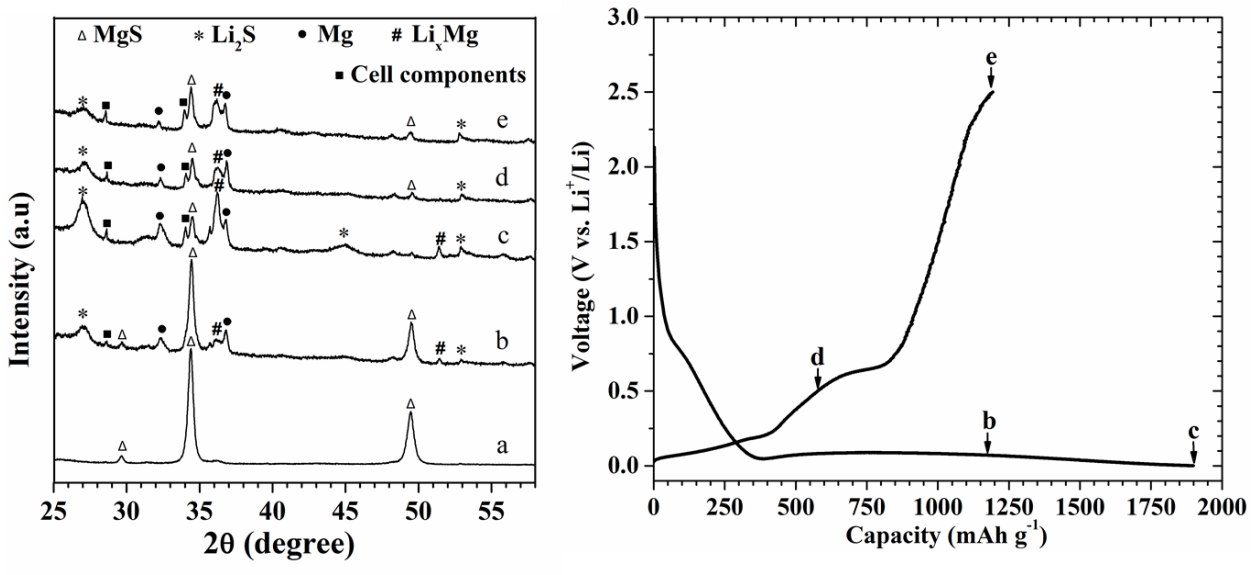

Fig. 3 XRD pattern of a) as-prepared MgS-CB and (b-e) *ex situ* XRD patterns of MgS-CB recorded at different points during the first discharge and charge processes.

The capacity contribution from Li_xMg alloy formation is approximately 600 mAh g^{-1}. This number is obtained from the first discharge curve after excluding the theoretical capacity of MgS from 1550 mAh g^{-1} (the contribution from the plateau between 0.1 and 0.001 V). However, the exact value of 'x' in Li_xMg alloy is difficult to deduce from the observed capacity as some amount of unreacted metallic Mg was observed after discharging to 0.001 V, cut off voltage. During charge, initially lithium is extracted from Li_xMg alloy and forms Mg metal. This is shown with an increase in intensity of Mg in Fig. 3d. Above 0.5 V, lithium is extracted from Li_2S and reacts with Mg to form MgS during this reaction the intensity of Mg is reduced (Fig. 3e). Though the intensity of Li_xMg seems to increase during this step, it is remaining constant only the intensity of Mg peak is changing (Fig 3d and 3e). From Fig. 3c and Fig. 3d, the peak intensities corresponding to Li_xMg alloy is reduced and from Fig. 3d and Fig. 3e the peak intensities corresponding to MgS is increased during charge further supporting the proposed mechanism.

The total charge capacity in the first cycle was 1200 mAh g^{-1}. After excluding the contribution from dealloying of Li_xMg (600 mAh g^{-1}, assuming full reversibility) from the total charge capacity, the remaining 600 mAh g^{-1} could be attributed to the delithiation of Li_2S. The

observed total capacity during charge proves the reversibility of Mg + Li_2S. The extraction of lithium occur in two steps one at 0.21 V which is in accordance with the extraction potential of lithium from Li-Mg alloy [32] and the second plateau centered at 0.6 V is due to the formation of MgS from Li_2S and Mg. The reversibility of magnesium based anode material is known from Mg + LiH system as reported by Tarascon group [21]. Based on the above experimental observations, the reversibility of Mg + Li_2S is concluded which is contrary to the mechanism proposed by Wang *et al* [30].

Though initial capacity of MgS is quite high, large irreversible capacity loss and a constant capacity fade over cycling were observed. During discharge and charge process it is evident that MgS is converted to Li_2S and Mg. This reaction is associated with a volume change of 85 %. This volume change leads to pulverization of active materials and hence significant amount of material will lose contact with carbon during cycling and restrain from contributing to the capacity. Inactive volume elements accumulate with cycling and hence capacity fades.

Further, ball milling of carbon can destroy and/or damage the carbon backbone and reduce the electronic conductivity, thereby contributing to capacity loss. To check this hypothesis and to enable electronic conductivity, MgS-CB composite was prepared with the addition of different conductive carbons. Electrodes were fabricated with 10 wt % of different conducting-carbons like carbon nanofibre (CNF), super P (SP) and graphene (Gra) in addition to as-prepared MgS-CB composite and binder. Though the initial capacity fading was not retrieved by addition of carbon (as it again implies the nature of ball milled sample) the cycling stability was significantly improved depending on the nature of the carbon added (Fig. 4a). This is substantiated by the impedance data shown in (Fig. 4b).

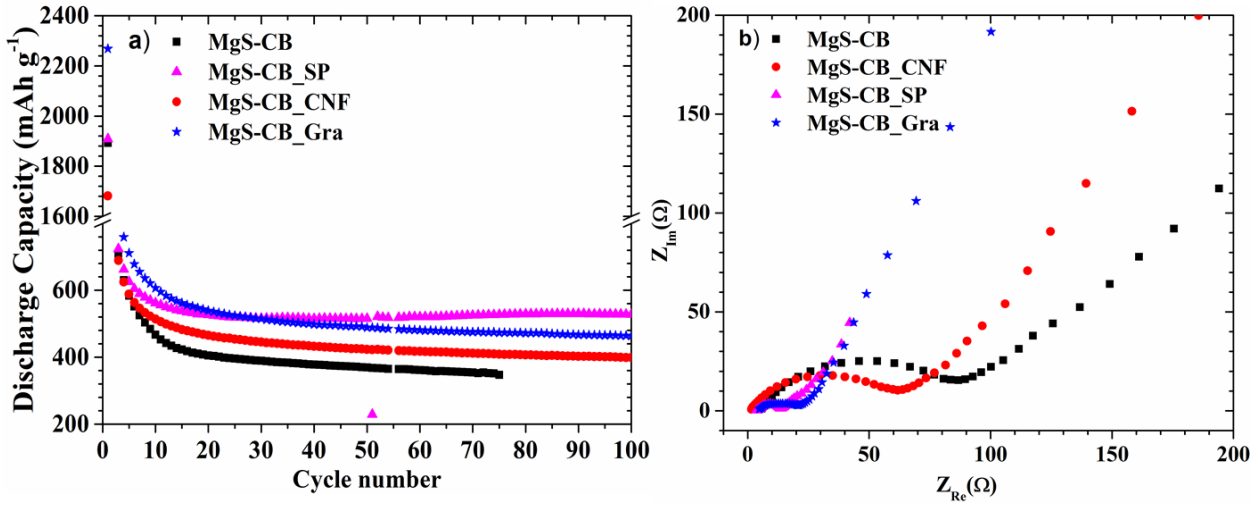

Fig. 4 (a) Cycling test for the cells with as-prepared MgS-CB electrode (50 mA g^{-1}) and different carbon containing MgS-CB electrodes measured at a constant current density of 100 mA g^{-1}. (b) Nyquist plots for cells with as-prepared MgS-CB electrode and different carbon containing MgS-CB electrodes recorded after 50 cycles.

Fig. 4a shows the variation of discharge capacities of samples with cycling tests. The total discharge capacity in the first cycle for as-prepared MgS-CB and MgS-CB with Gra, SP and CNF was 1899, 2268, 1909 and 1682 mAh g^{-1} respectively. The capacity contribution between OCV and 0.1 V for Gra, SP, CNF containing MgS-CB and the as-prepared MgS-CB are 672, 417, 337 and 318 mAh g^{-1} respectively. The variation in the discharge capacities are attributed to the SEI and lithium insertion into the respective carbon. Further, the MgS-CB with carbon additive exhibited improved cycling stability and reversible capacity with cycling numbers compared to as-prepared MgS-CB composite. In particular, MgS-CB with super P exhibited superior performance compared to graphene or CNF additive. A stable capacity of 530 mAh g^{-1} after 100 cycles was obtained for electrodes with super P compared to 470 mAh g^{-1} and 410 mAh g^{-1} in the case of electrodes with graphene and CNF respectively. To better understand the improved cycling stability of the carbon added MgS-CB, after 50 charge-discharge cycles the cells were examined using electrochemical impedance spectroscopy (EIS).

Fig. 4b shows the Nyquist plots for the cells with as-prepared MgS-CB and other conducting carbon added MgS-CB electrodes. All samples exhibited similar EIS spectra with a combination of a semicircle in high frequencies and a straight line at low frequencies. The

diameter of the semicircle attributed to interfacial charge transfer resistance (Rct) is decreased for conducting carbon added samples compared to as-prepared MgS-CB system. The intercepts with real impedance [Z_{Re}] axis of as prepared MgS-CB and CNF, Gra and SP containing MgS-CB were 94, 69, 24 and 14 Ohms respectively. Among various conducting carbon added MgS-CB, Super P incorporated MgS-CB exhibited low resistance hence, improved cycling stability and reversibility with cycling number (Fig. 4a). The order of decreased resistance among various carbon containing MgS-CB are consistent with cycling stability and reversibility. Hence it is likely that these improvements were promoted or enabled by the improved electronic conductivity which increased the effective electrochemical interface.

The practicality of as-prepared MgS anode was tested in full cells with lithium nickel manganese cobalt oxide (LNMC) and lithium iron phosphate (LFP) as cathode. The capacities were calculated with respect to the mass of LNMC (11.5 mg cm^{-2}) and LFP (10.8 mg cm^{-2}). The MgS-CB_SP electrodes were cycled to obtain a stable capacity in the half cell before employing for full cell studies. Fig. 5a shows the charge/discharge curves of LNMC vs. MgS cell and its cycling stability was plotted in Fig. 5b. The first charge capacity was 171 mAh g^{-1}. The first discharge capacity was 131 mAh g^{-1}. Large irreversible capacity was seen in the first cycle and a gradual fading in capacity was observed with cycling. Interesting feature of the LNMC vs. MgS cell is that the charge/discharge profiles are similar to that of LNMC vs. Li cells [39], only difference being the shift in the discharge voltage. Fig. 5c shows the charge/discharge profiles of LFP vs. MgS cells and its cycling behaviour is shown in Fig. 5d. A first charge capacity of 156 mAh g^{-1} was achieved and a first discharge capacity of 108 mAh g^{-1}. On subsequent cycling capacity faded gradually. The charge/discharge profiles are not flat in LFP vs. MgS cell compared to LFP vs Li cell [40] which is due to the nature of anode. In either case, capacity in the first charge is close to the theoretical capacity with respect to the cathode was achieved. On subsequent cycling, a constant capacity fading was observed. We believe that this capacity fading can be mitigated by optimizing the voltage window and by balancing the capacities of anode and cathode.

4. Conclusions

MgS-carbon composite was synthesized and investigated as a potential low voltage anode material for lithium-ion batteries. Based on voltage-capacity profiles and ex-situ XRD studies a reversible lithiation and delithiation mechanism for MgS is concluded. With a first optimized electrode fabrication a stable capacity of 530 mAh g^{-1} was obtained. Further, the feasibility of MgS carbon composite as anode material vs lithium nickel manganese cobalt oxide (LNMC) and lithium iron phosphate (LFP) cathode were tested. We believe that by adopting a different preparation method a highly reversible anode material can be realized. Such studies are underway.

Acknowledgments

Financial support by the EU project "Hi-C", grant # 608575 is gratefully acknowledged.

References

[1] J-M.Tarascon, M. Armand, Issues and Challenges Facing Rechargeable Lithium Batteries, Nature 414 (2001) 359-367.
[2] A.S. Arico, P. Bruce, B. Scrosati, J-M.Tarascon, W. van Schalkwijk, Nanostructured Materials for Advanced Energy Conversion and Storage Devices, Nat. Mater. 4 (2005) 366-377.
[3] M. Armand, J-M.Tarascon, Building Better Batteries, Nature 451 (2008) 652-657.
[4] R.A. Huggins, Lithium alloy negative electrode, J. Power Sources 81–82 (1999) 13–19.
[5] J.B. Goodenough, Y. Kim, Challenges for Rechargeable Li Batteries , Chem. Mater.22 (2010) 587–603.
[6] L. Ji, Z. Lin, M. Alcoutlabi, X. Zhang, Recent Developments in Nanostructured Anode Materials for Rechargeable Lithium-Ion Batteries, Energy Environ. Sci.4 (2011) 2682-2699.
[7] N.P. Yao, L.A. Heredy, R.C. Saunders, Emf Measurements of Electrochemically Prepared Lithium-Aluminum Alloy, J. Electrochem. Soc. 118 (1971) 1039-1042.
[8] Y. Hamon, T. Brousse, F. Jousse, P. Topart, P. Buvat, D.M. Schleich, Aluminum Negative Electrode in Lithium Ion Batteries, J. Power Sources 97 (2001) 185-187.

[9] J. Wang, I.D. Raistrick, R.A. Huggins, Behavior of Some Binary Lithium Alloys as Negative Electrodes in Organic Solvent-Based Electrolytes, J. Electrochem. Soc. 133 (1986) 457-460.
[10] M. Winter, J.O. Besenhard, Electrochemical Lithiation of Tin and Tin-Based Intermetallics and Composites, Electrochim. Acta 45 (1999) 31-50.
[11] J. Yang, M. Winter, J.O. Besenhard, Small Particle Size Multiphase Li-Alloy Anodes for Lithium-Ion-Batteries, Solid State Ionics 90 (1996) 281-287.
[12] S. Bourderau, T. Brousse, D.M. Schleich, Amorphous Silicon as a Possible Anode Material For Li-Ion Batteries, J. Power Sources 81-82 (1999) 233–236.
[13] T.D. Hatchard, J.R. Dahn, In Situ XRD and Electrochemical Study of the Reaction of Lithium with Amorphous Silicon, J. Electrochem. Soc. 151 (2004) A838-A842.
[14] H. Wu,Y. Cui, Designing Nanostructured Si Anodes for High Energy Lithium Ion Batteries, Nano Today 7 (2012) 414–429.
[15] J. Graetz, C.C. Ahn, R. Yazami, B. Fultz, Nanocrystalline and Thin Film Germanium Electrodes with High Lithium Capacity and High Rate Capabilities, J. Electrochem. Soc.151 (2004) A698-A702.
[16] M-H. Park, Y. Cho, K. Kim, J. Kim, M. Liu, J. Cho, Germanium Nanotubes Prepared by Using the Kirkendall Effect as Anodes for High-Rate Lithium Batteries, Angew. Chem. Int. Ed. 50 (2011) 9647-9650.
[17] P. Poizot, S. Laruelle, S. Grugeon, L. Dupont, J.M. Tarascon, Nano-Sized Transition-Metal Oxides as Negative-Electrode Materials for Lithium-Ion Batteries, Nature 407 (2000) 496-499.
[18] M.V. Reddy, G.V.S. Rao, B.V.R. Chowdari, Metal Oxides and Oxysalts as Anode Materials for Li Ion Batteries, Chem. Rev. 113 (2013) 5364–5457.
[19] H. Li, P. Balaya, J. Maier, Li-Storage via Heterogeneous Reaction in Selected Binary Metal Fluorides and Oxides, J. Electrochem. Soc. 151 (2004) A1878-A1885.
[20] C-M Park, J-H Kim, H. Kim, H-J.Sohn, Li-Alloy Based Anode Materials for Li Secondary Batteries, Chem. Soc. Rev. 39 (2010) 3115-3141.
[21] Y. Oumellal, A. Rougier, G.A. Nazri, J.M. Tarascon, L. Aymard, Metal Hydrides for Lithium-Ion Batteries, Nat. Mater. 7 (2008) 916-921.
[22] G.X. Wang, S. Bewlay, J. Yao, H.K. Liu, S.X. Dou, Tungsten Disulfide Nanotubes for Lithium Storage, Electrochem. Solid-State Lett.7 (2004) A321-A323.

[23] M.S. Whittingham, Chemistry of Intercalation Compounds: Metal Guests in Chalcogenide Hosts, Prog. Solid St. Chem. 12 (1978) 41-99.
[24] M. Nishijima, T. Kagohashi, M. Imanishi, Y. Takeda, O. Yamamoto, S. Kondo, Synthesis and Electrochemical Studies of a New Anode Material, $Li_{3-x}Co_xN$, Solid State Ionics83 (1996) 107-111.
[25] T. Shodai, S. Okada, S. Tobishima, J. Yamaki, Anode Performance of a New Layered Nitride $Li_{3-x}Co_xN$ (x = 0.2–0.6), J. Power Sources 68 (1997) 515-518.
[26] D.C.S. Souza, V. Pralong, A.J. Jacobson, L.F. Nazar, A Reversible Solid-State Crystalline Transformation in a Metal Phosphide Induced by Redox Chemistry, Science 296 (2002) 2012-2015.
[27] F. Gillot, L. Monconduit, M. Morcrette, M.L. Doublet, L. Dupont, J-M.Tarascon, On the Reactivity of $Li_{8-y}Mn_yP_4$ toward Lithium , Chem. Mater. 17 (2005) 3627-3635.
[28] J. Cabana, L. Monconduit, D. Larcher, M.R. Palacín, Beyond Intercalation-Based Li-Ion Batteries: The State of the Art and Challenges of Electrode Materials Reacting Through Conversion Reactions, Adv. Mater. 22 (2010) E170–E192.
[29] X.H. Liu, L. Zhong, S. Huang, S.X. Mao, T. Zhu and J.Y. Huang, Size-Dependent Fracture of Silicon Nanoparticles During Lithiation, ACS Nano 6 (2012) 1522-1531.
[30] M. Wang, X. Li, M. Gao, H. Pan, Y. Liu, A Novel Synthesis of MgS and its Application as Electrode Material for Lithium-Ion Batteries, J Alloy Compd. 603 (2014) 158–166.
[31] N. Singh, D.R. Vij, Luminescence and Related Properties of Magnesium Sulphide Phosphors, J. Mater. Sci. 29 (1994) 4941-4945.
[32] Z. Shi, M. Liu, D. Naik, J. L. Gole, Electrochemical Properties of Li–Mg Alloy Electrodes for Lithium Batteries, J. Power Sources, 92 (2001)70-80.
[33] C-M. Park, Y-U. Kim, H. Kim, H-J. Sohn, Enhancement of the Rate Capability and Cyclability of an Mg–C Composite Electrode for Li Secondary Batteries, J. Power Sources 158 (2006) 1451-1455.
[34] H. Kim, B. Park, H.-J. Sohn, T. Kang, Electrochemical Characteristics of Mg–Ni Alloys as Anode Materials for Secondary Li Batteries, J. Power Sources, 90 (2000) 59-63.
[35] H. Kim, J. Choi, H.-J. Sohn, T. Kang, The Insertion Mechanism of Lithium into Mg2Si Anode Material for Li-Ion Batteries, J. Electrochem. Soc., 146 (1999), p. 4401-4405.

[36] H. Kim, Y.-J. Kim, D.G. Kim, H.-J. Sohn, T. Kang, Mechanochemical Synthesis and Electrochemical Characteristics of Mg2Sn as an Anode Material for Li-Ion Batteries, Solid State Ionics, 144 (2001), p. 41-49.
[37] M. Winter, P. Novák, A. Monnier, Graphites for Lithium-Ion Cells: The Correlation of the First-Cycle Charge Loss with the Brunauer-Emmett-Teller Surface Area, J. Electrochem. Soc. 145 (1998) 428-436
[38] M. Jagannathan, K.S.R. Chandran, Electrochemical Charge/Discharge Behavior and Phase Transitions during Cell Cycling of Li(Mg) Alloy Anodes for High Capacity Li Ion Batteries, J. Electrochem. Soc. 160 (2013) A1922-A1926.
[39] B. J. Hwang, Y. W. Tsai, D. Carlier, G. Ceder, A Combined Computational/Experimental Study on $LiNi_{1/3}Co_{1/3}Mn_{1/3}O_2$, Chem. Mater. 15 (2003) 3676-3682.
[40] A. K. Padhi, K. Nanjundaswamy, J. B. Goodenough, Phospho-olivines as Positive-Electrode Materials for Rechargeable Lithium Batteries, J. Electrochem. Soc. 144 (1997) 1188-1194.

Figure Captions

Fig. 1 SEM images of as-prepared MgS-CB and the corresponding EDS mapping of Mg, S and C.

Fig. 2 Electrochemical properties of MgS-CB prepared by ball milling. (a) Cyclic voltammogram of MgS-CB at a scan rate of 0.03 mV s^{-1}. (b) The discharge and charge profiles of MgS-CB obtained at 50 mA g^{-1}.

Fig. 3 XRD pattern of a) as-prepared MgS-CB and (b-e) ex situ XRD patterns of MgS-CB recorded at different points during the first discharge and charge processes.

Fig. 4 (a) Cycling test for the cells with as-prepared MgS-CB electrode (50 mA g^{-1}) and different carbon containing MgS-CB electrodes measured at a constant current density of 100 mA g^{-1}. (b)

Nyquist plots for cells with as-prepared MgS-CB electrode and different carbon containing MgS-CB electrodes recorded after 50 cycles.

Fig. 5 Full cell performance of cycled MgS-CB_SP as anode with lithium nickel manganese cobalt oxide (LNMC) and lithium iron phosphate (LFP) as cathode